On Dark Peaks and Missing Mass: A Weak-lensing Mass Reconstruction of the Merging Cluster System A520

D. Clowe[1], M. Markevitch[2], M. Bradac[3], A. Gonzalez[4], S. Chung[4], R. Massey[5], and D. Zaritsky[6]

1: 1 Department of Physics and Astronomy, Ohio University, 251B Clippinger Labs, Athens, OH 45701, USA
2: NASA Goddard Space Flight Center, Code 662, 8800 Greenbelt Road, Greenbelt, MD 20706, USA
3: Department of Physics, University of California, One Shields Avenue, Davis, CA 95616, USA
4: Department of Astronomy, University of Florida, 211 Bryant Space Science Center, Gainesville, FL 32611, USA
5: Department of Physics, Durham University, South Road, Durham DH1 3LE, UK
6: Steward Observatory, University of Arizona, 933 North Cherry Avenue, Tucson, AZ 85721, USA

18 de abril de 2013

Seminário do grupo de Extragaláctica

Departamento de Astronomia - IAG/USP

Sumário

Abell 520

- $z \sim 0.199$;
- Mahdavi+07: dark peak;
- Okabe & Umetsu 08: in agreement with Mahdavi+07;
- Jee+12;
- Clowe+12.

Mahdavi+07

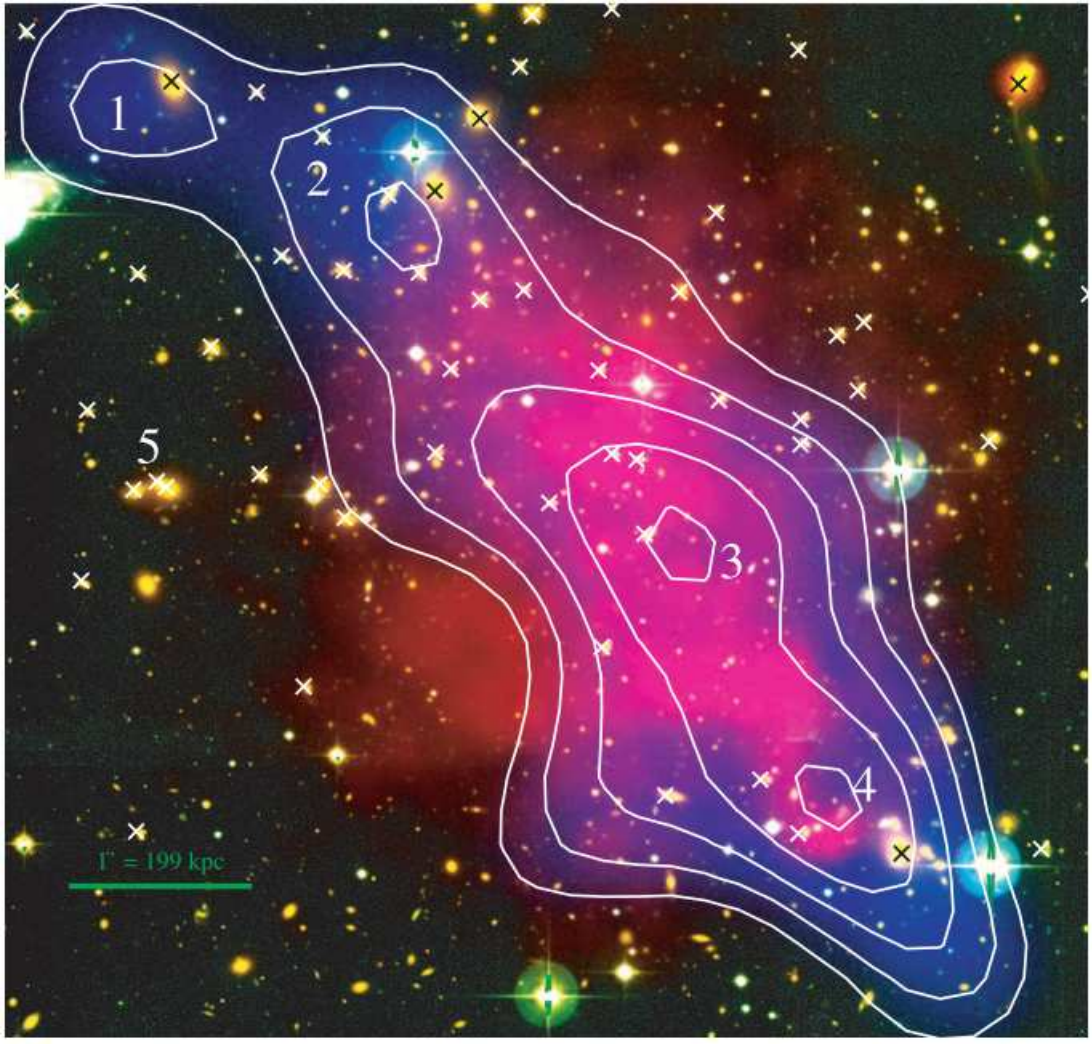

Central 6.4' $\times$ 6.4' of Abell 520, showing the CFHTimage, the diffuse Chandra X-ray emission (red), and the lensing surface mass density (blue, + 3, 3.5, 4, 4.5, and 5 σ contours determined from a bootstrap analysis). Spectroscopically confirmed member galaxies are marked with crosses; red-sequence galaxies appear orange.

Mahdavi+07

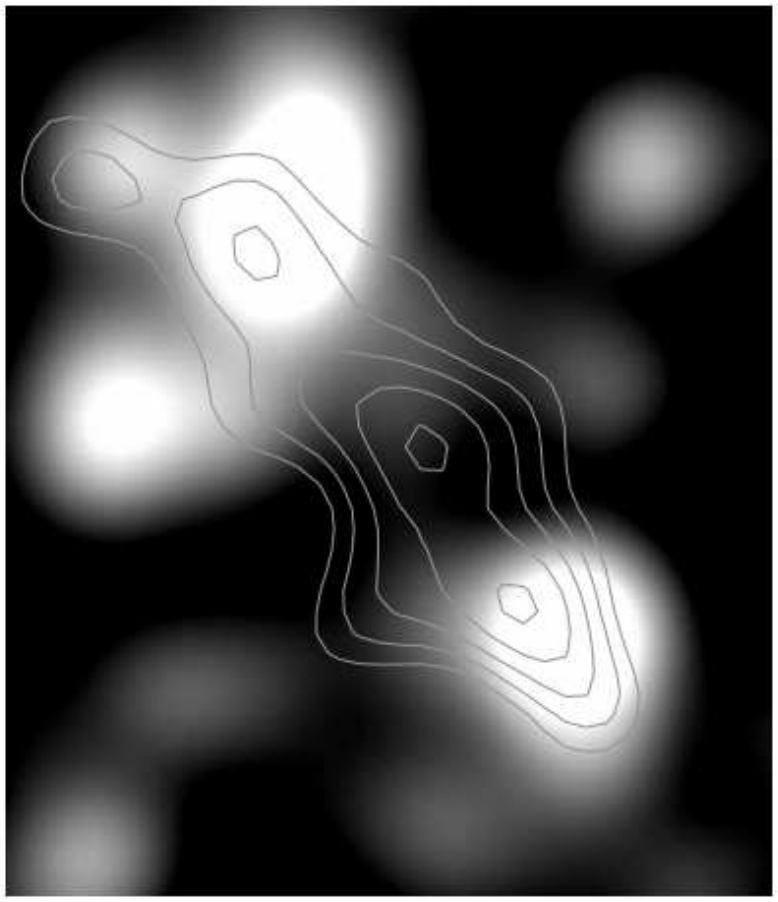

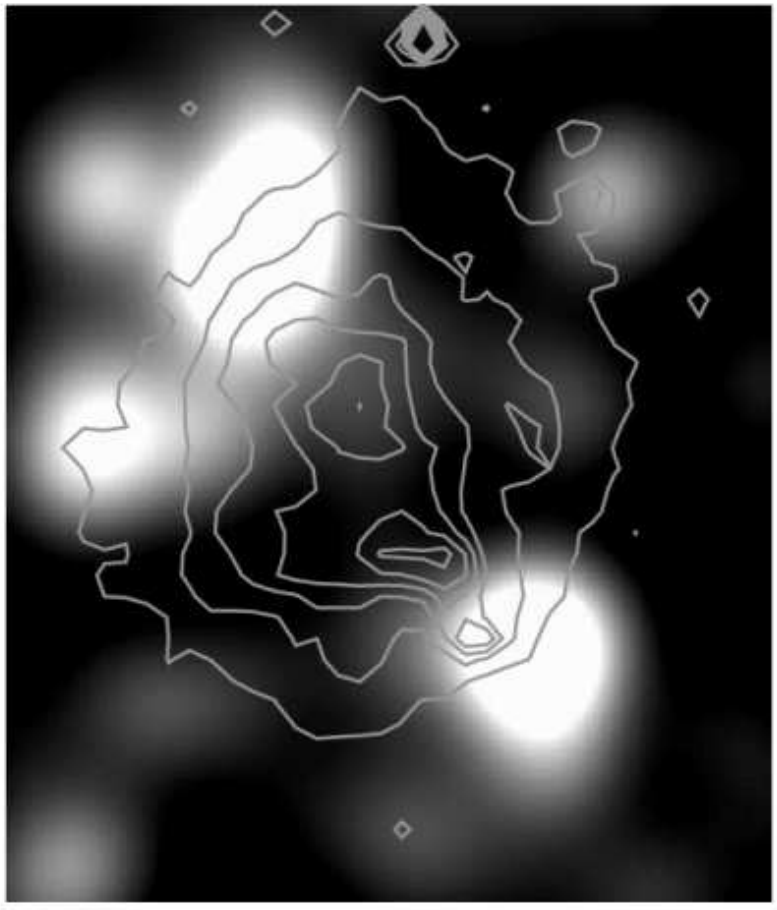

Red light distribution together with lensing contours from (a). (c) Same as (b), but with X-ray contours. Note the absence of galaxies in the central lensing peak.

Okabe & Umetsu 08

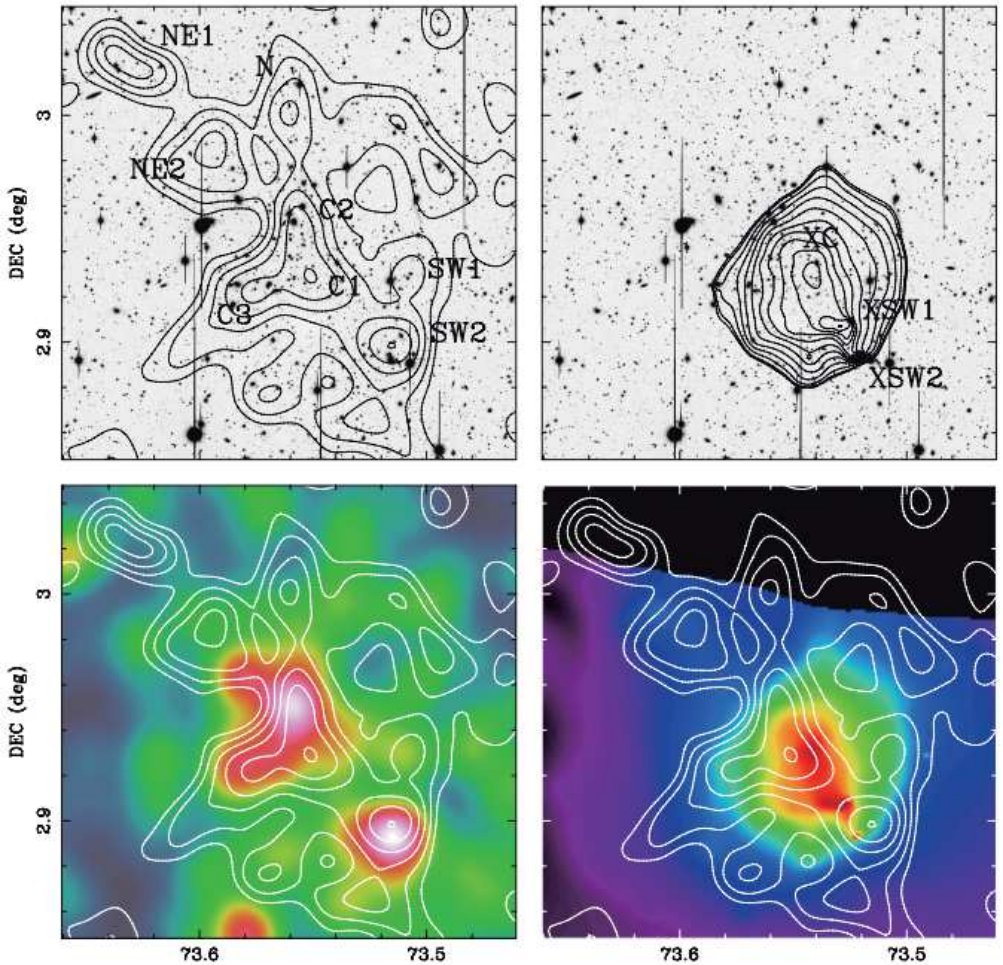

A520 Top-left: Subaru i'-band image of the central $\sim$ 12' $\times$ 12' cluster region. Overlaid are contours of the lensing κ-field reconstructed from weak shear data. The contours are spaced in units of 1σ reconstruction error. The Gaussian FWHM used for the mass reconstructions 1'.25. Top-right: adaptively-smoothed Chandra X-ray contours (0.7-7.0 keV) overlaid on the same i'-band image. Bottom-left: Cluster luminosity density distribution in the i'-band smoothed to the same angular resolution of the mass map. Overlaid are the same mass contours as in the top-left panel. Bottom-right: The same mass contours overlaid on the adaptively-smoothed Chandra X-ray image (0.7-7.0 keV).

Jee+12

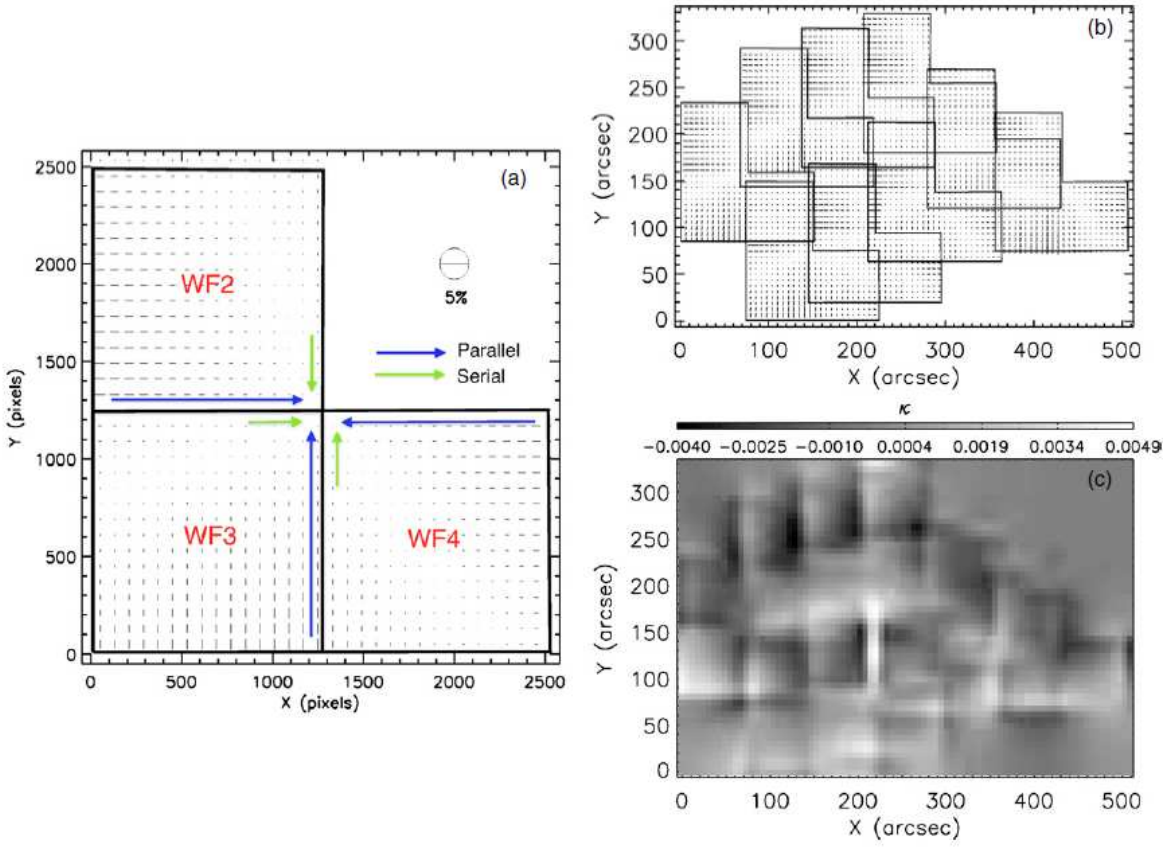

Influence of CTI on mass reconstruction. (a) CTI pattern within WFPC2 CCDs. It shows how typical circular WFPC2 PSFs are distorted due to CTI. The size and orientation of the 'whiskers' represent the magnitude and direction of elongation, respectively. (b) CTI-induced ellipticity pattern when the observational footprint is considered. (c) CTI-only mass reconstruction. The periodic variation due to the observational dither pattern is clear. However, even the maximum amplitude of the uncorrected systematics for the average source galaxy is an order of magnitude smaller than the average lensing signal.

Jee+12

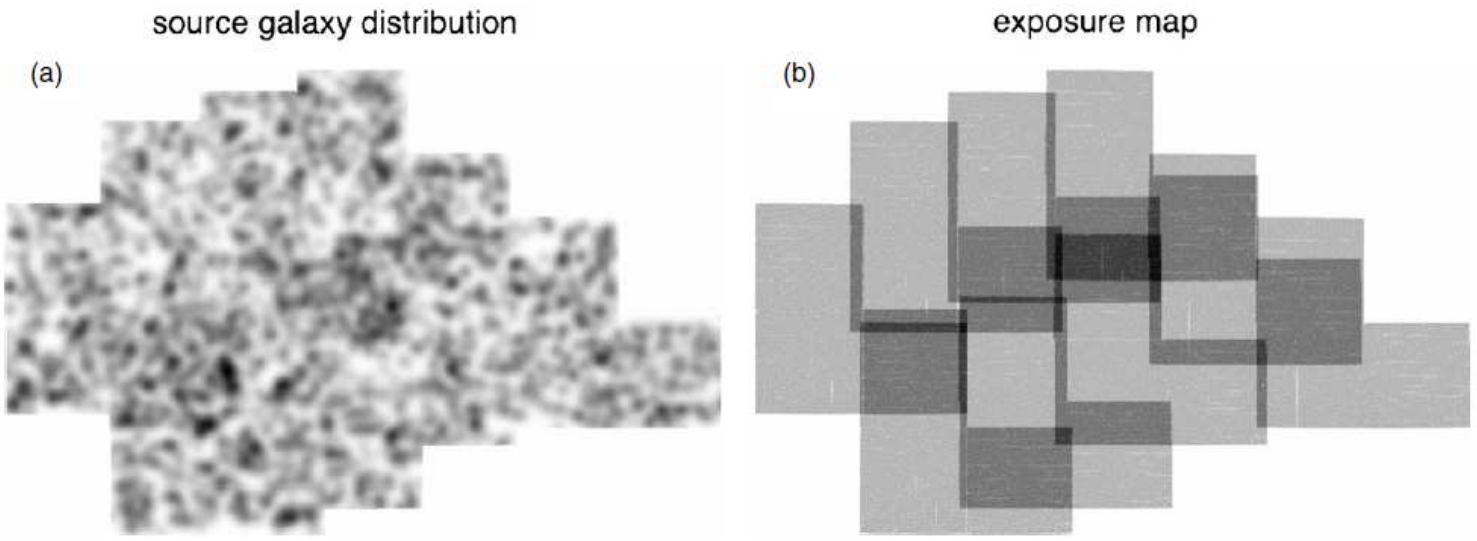

Source galaxy distribution vs. exposure map. Darker shade represents higher value. (a) Source galaxy positions are smoothed with an FWHM = 10” Gaussian kernel. (b) Shown here is the exposure map for the combined WFPC2 F814W image. The comparison of the two figures hints at the correlation between the image depth and number density of source galaxies. However, the correlation is not strong. On a 1’ scale (the size of WF CCD), the peak-to-valley source galaxy number density variation is at the $\sim$ 7% level with respect to the mean density whereas the exposure time varies significantly from $\sim$ 4400 s to 13200 s. Therefore, the spatial variation of the source galaxy number density due to the exposure time variation does not cause any spurious substructures in our mass reconstruction.

Jee+12

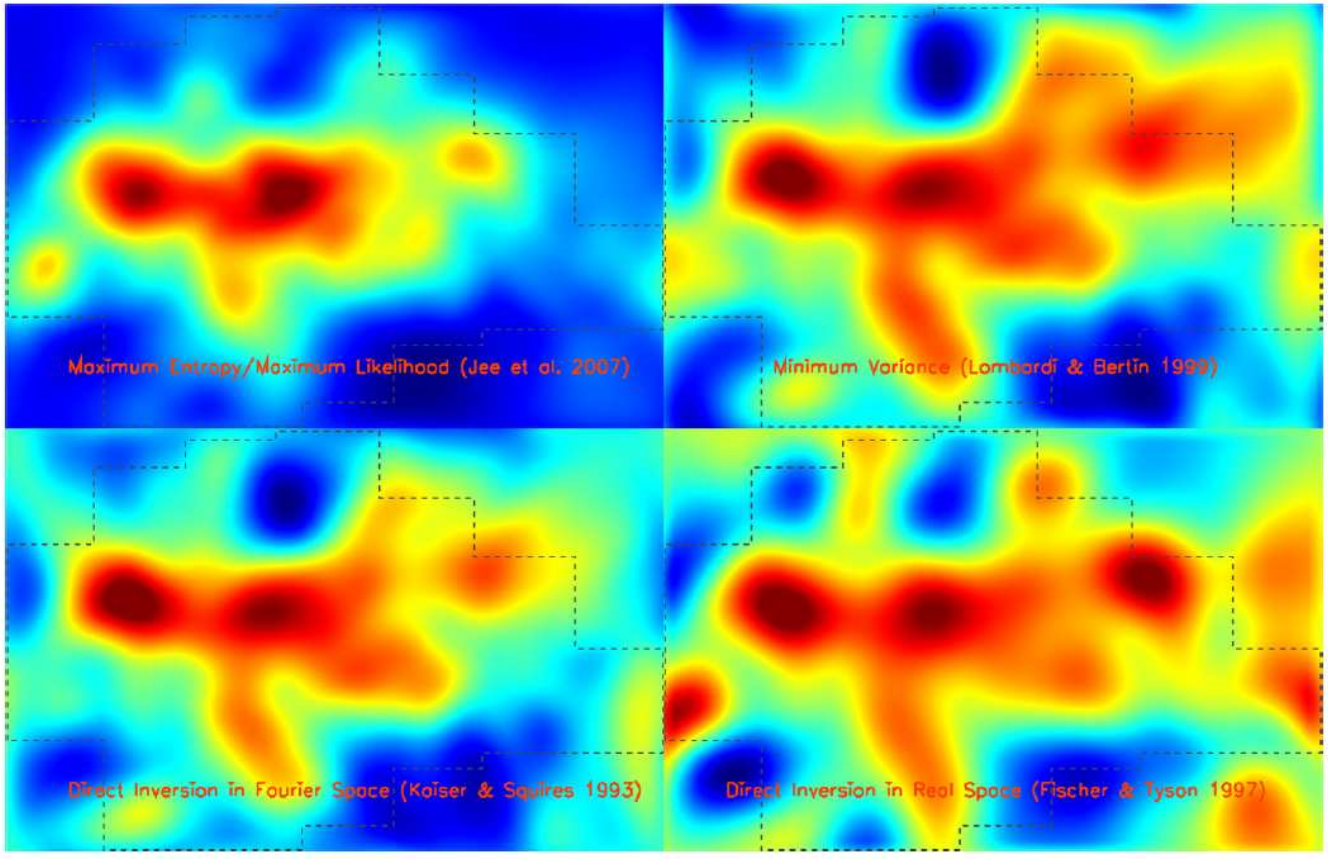

Mass reconstruction in A520 with different algorithms. The dashed line shows the footprint of the WFPC2 observations. The structures well inside the boundary are all visible in different algorithms whereas the structures near and outside the boundary depend on the reconstruction algorithms

Jee+12

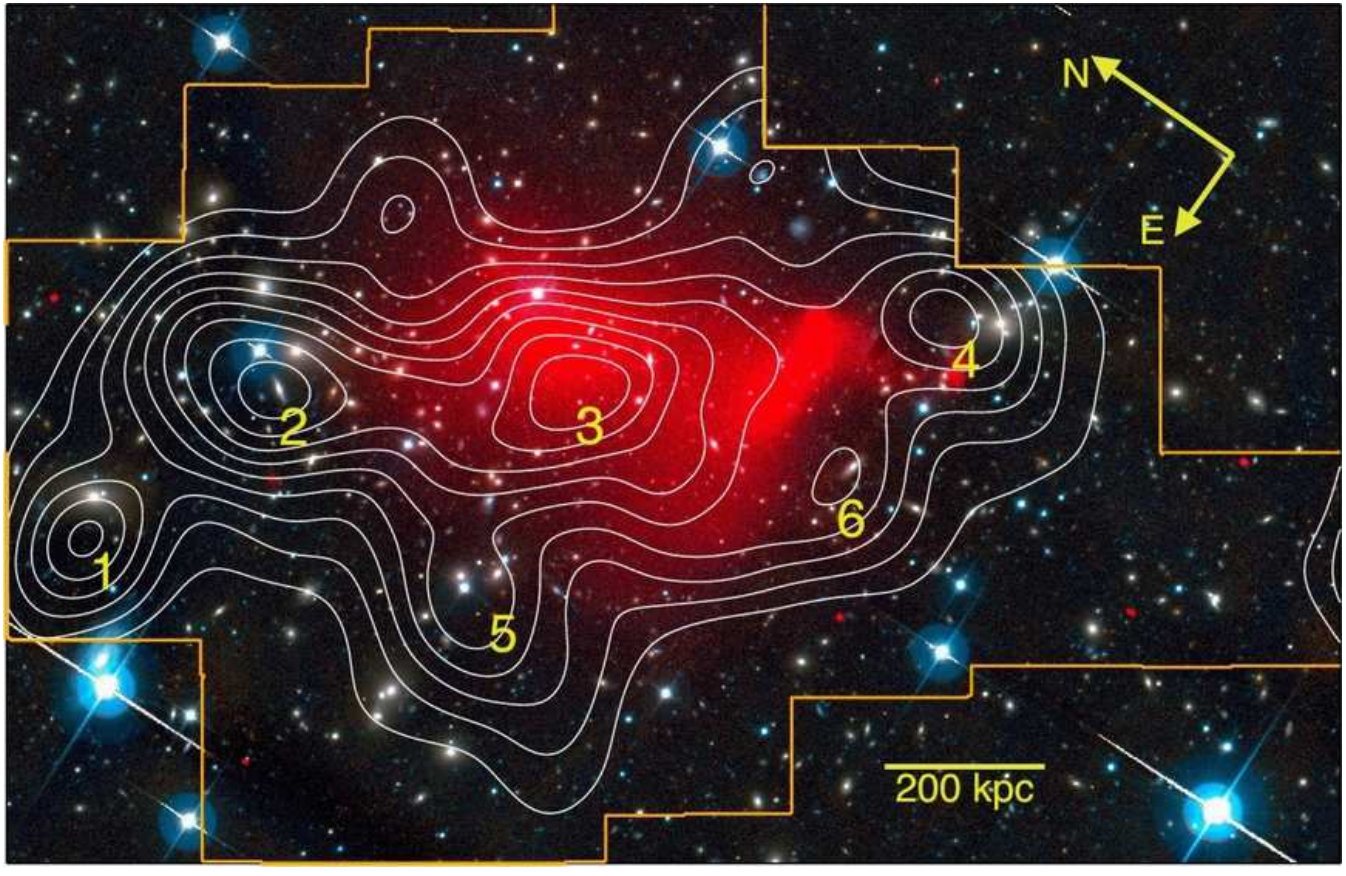

Mass reconstruction in A520. The intensity of the diffuse Chandra emission is depicted in red. The background is the pseudo-color composite created from the CFHT r and g passband images. The WFPC2 observation footprint is shown in orange. The white contours represent the convergence and the spacing is linear. The lowest contour corresponds to the $\sim 2.6\sigma$ significance. The numbers (1-6) indicate the significant mass peaks.

Jee+12

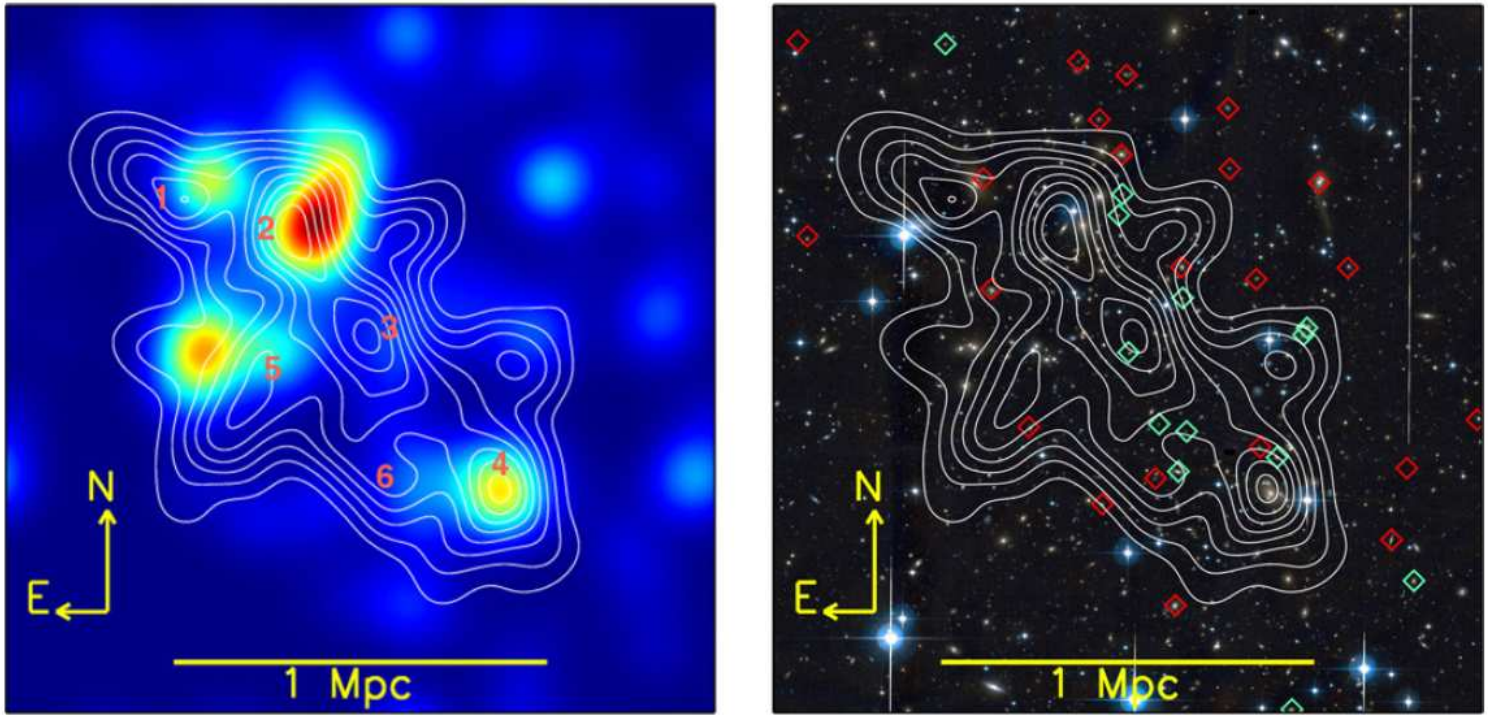

Large-field mass reconstruction based on the combined (HST and CFHT) catalogs. On the left-hand side, we overlay the mass contours on the smoothed restframe B-band luminosity distribution of the cluster (linear scale). On the right-hand side, we illustrate the distribution of the high (red diamond, δv_{rf} > 1700 km s^{-1}) and low (green diamond, δv_{rf} < -1500 km s^{-1}) velocity groups.

A dark peak?

- These results have also been used by several authors to argue in favor of an alternative gravity model (Moffat & Toth 09; Bekenstein 10);
- But, is not the first time (e.g. Abell 1942 [Erben+00] and Miralles+02);
- In both cases, the significance of the detections, as measured by the likelihood that a randomly chosen set of galaxies within the survey area would have a similar correlation in their orientations on the sky, was sufficiently large that one would not expect to find such systems by chance;
- However, in both cases, deeper observations resulted in the measurement of fainter galaxies that do not have the same correlated orientation, and therefore in the new analyses the mass overdensities either greatly diminished in amplitude (in the case of A1942; von der Linden+06) or completely vanished (in the case of the STIS dark lens; Erben+03).

Clowe+12

- Magellan (much longer exposure times) + HST-ACS (deeper than the WFPC2 mosaic + 3 colours);
- During its $\sim$ 10 years above the protection of the Earth's atmosphere, ACS has accumulated significant radiation damage that has degraded its CCD detectors.
- After each exposure, as photoelectrons are transferred through the silicon substrate to the readout electronics, a certain fraction is temporarily retained by lattice defects created by the radiation damage, and released after a short delay (Janesick 2001).
- This effect is known as charge transfer inefficiency (CTI) and spuriously elongates the shapes of (in particular) faint galaxies in a way that mimics weak gravitational lensing

HST

- Correction: 2 independent pipelines;
- The resulting weak-lensing shear measurements for the two CTI correction pipelines were consistent within 1% of each other, in agreement with our estimate of the expected residual shear from the CTI correction.
- At this level there is minimal effect on the weak-lensing mass measurements presented herein.

Magellan

- IMACS camera;
- During this time there were two significant problems with IMACS: The atmospheric distortion corrector had not yet been delivered to the telescope, and a problem with the CCD amplifiers created horizontal streaking in images after a saturated pixel was read;
- As a result, while many of the images were obtained with $\sim$0“.6 seeing, they had 1”.0 effective seeing at the edges of the image, $\sim$ 8’ from the center, and 1“.4 seeing with noticeable coma in the corners of the images;
- We therefore left it in the images, being sure to mask any streaks prior to the creation of flat fields and removed any galaxies that overlapped a streak from our weak-lensing galaxy catalog.
- Bessel B, V, and R;
- Final integration times were 120 minutes in R and 40 minutes each in B and V.
- Seeing varied between $0.5 - 0.7$ in the R images, $0.7 - 0.9$ in the V images, and $\sim$ 1.0 in the B images.

R-X images

- We have created an approximate projected gas mass map using a 0.8-4 keV X-ray image extracted from the archival Chandra 520 ks data set;

Weak lensing

- Weak-lensing analysis is done by measuring second moments of the surface brightness to calculate an ellipticity for each galaxy, correcting this shape for smearing by the PSF to measure a shear, rejecting stars by size and central surface brightness, and rejecting likely cluster and foreground galaxies by color.
- The methodology we use for the PSF correction is that of a modified KSB technique (Kaiser+95);
- Galaxies selected for the weak-lensing analysis had a photometric S/N > 10 in the R or F814W passbands,R > 22 or F814W > 21.5, and did not have any bright neighbors near enough to significantly influence the second moment measurements (less than three times the sum of the scale radii of the galaxy and the neighbor).
- Weak-lensing analysis is performed separately on the co-added Magellan image and on each of the four ACS pointings, then we combine the resulting shear catalogs to produce a final catalog.

Weak lensing

- The weak lensing measurements were performed with a modified versionof the IMCAT8 software package;
- Because the HST and Magellan images observe galaxy populations with different redshift distributions,we need to adjust the catalogs to have the same mean lensing depth;
- Using external photometric redshift catalogs , we determined that the HST data set would have a mean lensing signal in a given region that is 1.05 $\times$ that of the Magellan image. We therefore scale the shears measured in the Magellan image by 1.05 before combining with the HST catalog to create the final weak-lensing catalog;
- The final lensing catalog has a number density of galaxies of 22 arcsec^{-2} for the Magellan images and 56 for the ACS images.

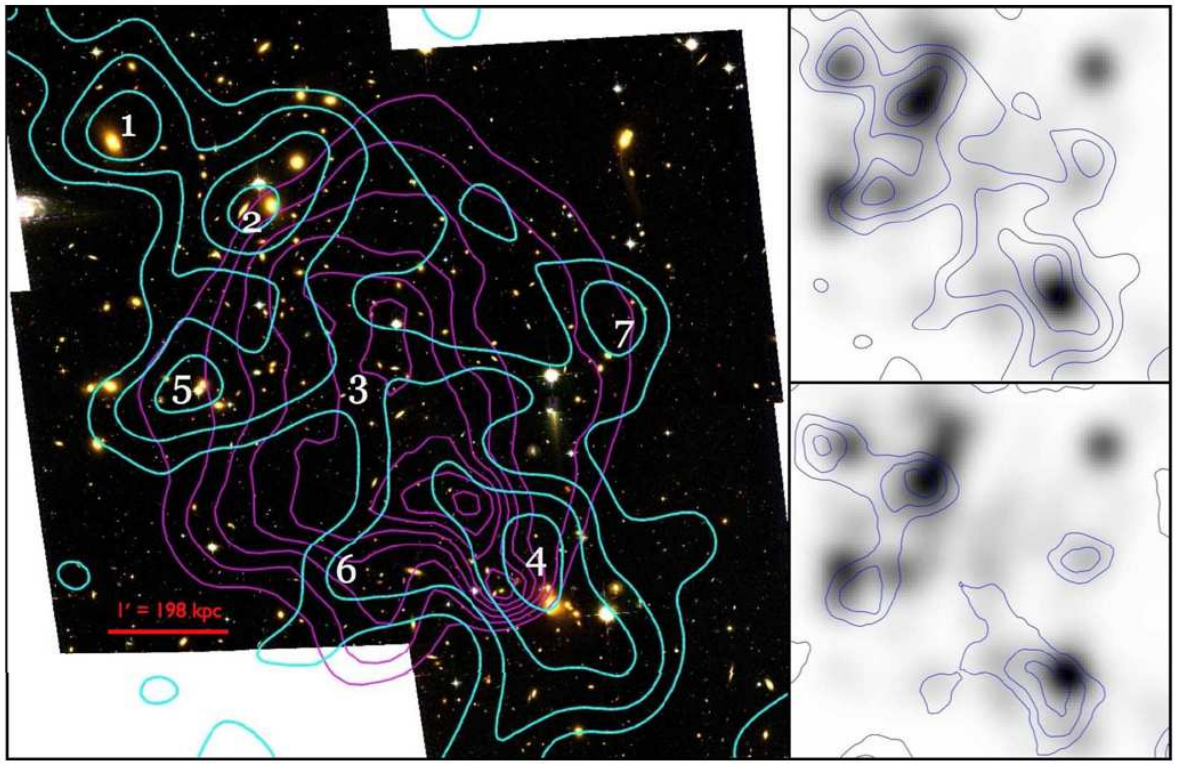

Left panel shows a 7’ $\times$ 6’ 75 color composite from the HST ACS mosaic images with the weak-lensing surface density reconstruction overlaid in cyan contours and the Chandra X-ray-derived gas surface density in magenta contours. The weak-lensing contours show steps in surface density of 2×10^8 $M_\odot$ kpc^{-2} (κ steps of 0.056) above the mean surface mass density at the edge of the Magellan image ($\sim$ 1600 kpc radius), and the gas mass contours showsteps of 7.4×10^6 $M_\odot$ kpc^{-2} with the outer contour starting at 4.4×10^7 $M_\odot$ kpc^{-2}. The upper right panel shows the weak-lensing contours superimposed on a smoothed cluster galaxy luminosity distribution in gray scale, with both the luminosity and surface density distributions smoothed by the same σ = 60 kpc Gaussian kernel. The bottom-right panel shows contours of the mass aperture statistic from the weak-lensing data, with contours of steps of 1σ, superimposed on the cluster galaxy luminosity distribution. Also labeled in the left panel are the regions of structures 1-6 identified in M07 and J12, as well as the new structure 7.

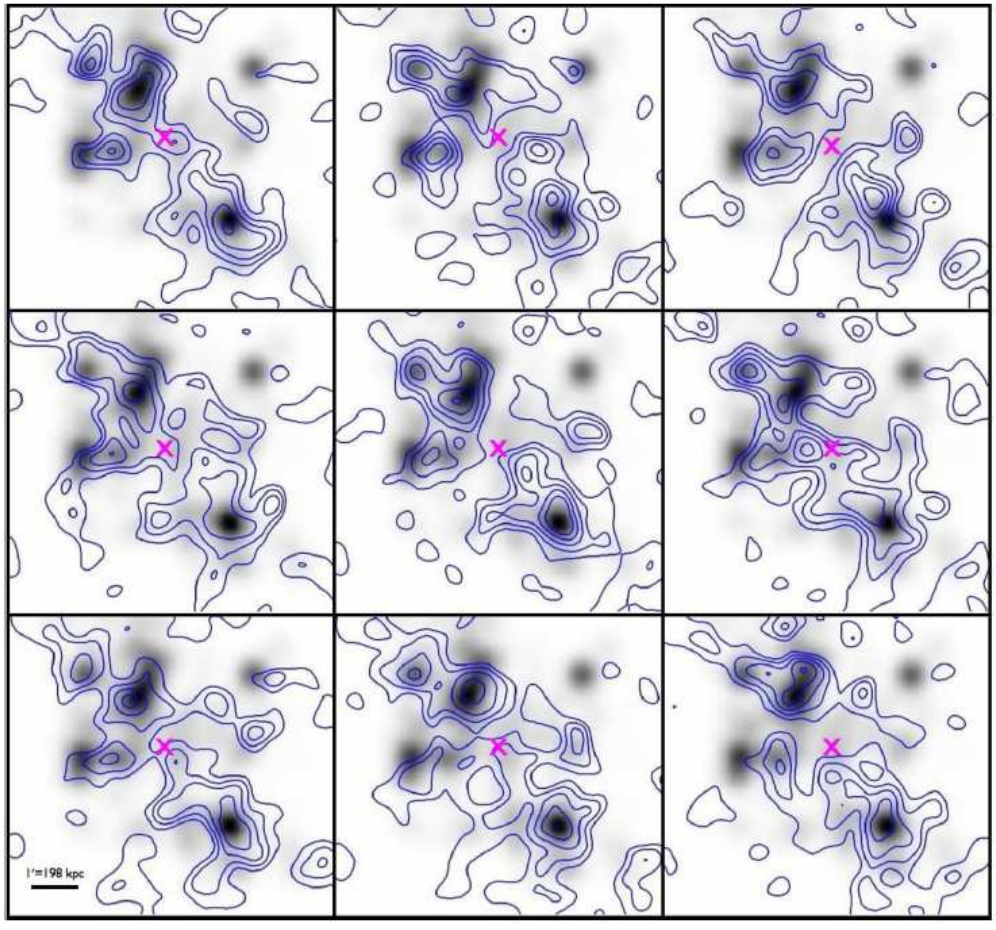

Nine randomly selected weak-lensing surface density reconstructions from the 100000 bootstrap resampled catalogs used to measure errors in the weaklensing reconstructions superimposed on the cluster galaxy luminosity distribution. The contour levels are identical to those in Figure 2, and the magenta $\times$ shows the location of the dark peak of J12 (structure 3). The middle-right reconstruction shows a structure that is morphologically similar to and has similar mass as the dark peak in J12; such structures are found in $\sim$2% of the bootstrap resampled reconstructions, and are the only reconstructions in which the column mass in the dark peak location agrees with that of J12. Other reconstructions show smaller peaks near the dark peak, but have much less mass than reported by J12.

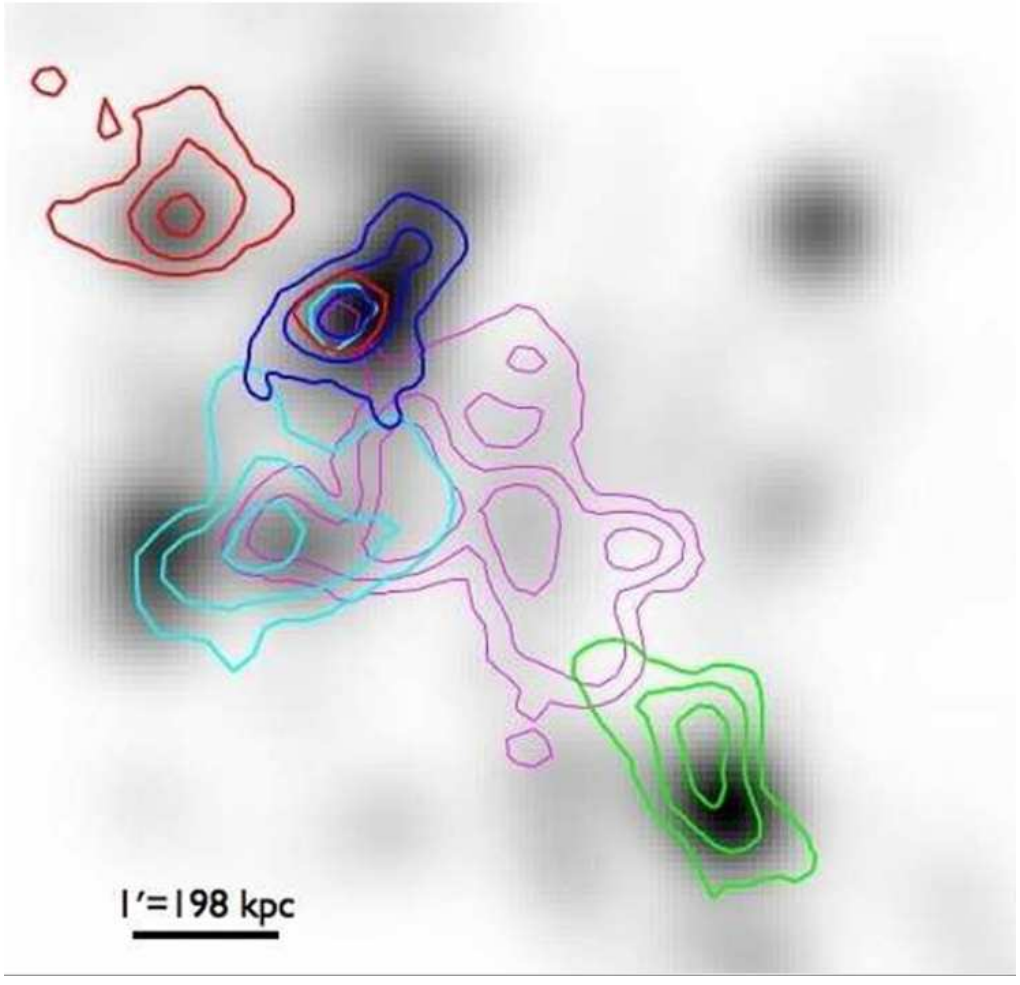

Contours enclosing the mass centroid position uncertainties for structures 1 (red), 2 (blue), 3 (magenta), 4 (green), and 5 (cyan) superimposed on the cluster galaxy luminosity in gray scale. The contours enclose the locations of the detected mass centroids in 100,000 bootstrap resamplings of the reduced shear catalog, and encompass 68%, 95%, and 99.7% of the centroid measurements.

Mass Reconstruction Substructure Properties ($r < 150\,\mathrm{kpc}$)

Substructure	R.A. (h : m : s)	Decl. (° : ′ : ″)	Column Mass ($h_{70}^{-1}\,10^{13}\,M_{\odot}$)	Luminosity ($h_{70}^{-2}\,10^{11}\,L_{z\odot}$)	Gas Mass ($h_{70}^{-5/2}\,10^{13}\,M_{\odot}$)	M/L ($M_{\odot}/L_{z\odot}$)
P1	04:54:19.60	+02:57:49.09	3.03 ± 0.69	2.43	0.25	114 ± 28
P2	04:54:14.84	+02:57:06.25	4.08 ± 0.73	4.16	0.40	88 ± 18
P3	04:54:11.25	+02:55:37.28	2.26 ± 0.75	1.38	0.69	114 ± 54
P4	04:54:04.57	+02:53:58.60	4.64 ± 0.63	3.11	0.50	133 ± 20
P5	04:54:17.11	+02:55:30.09	3.00 ± 0.77	2.66	0.44	96 ± 29
P6	04:54:09.61	+02:53:55.90	3.03 ± 0.66	1.15	0.65	207 ± 57

Aperture Densitometry Substructure Properties ($r < 150\,\mathrm{kpc}$)

Substructure	ζ Column Mass ($h_{70}^{-1}\,10^{13}\,M_\odot$)	$M/L\,(\zeta)$ ($M_\odot/L_{z\odot}$)	ζ_c Column Mass ($h_{70}^{-1}\,10^{13}\,M_\odot$)	$M/L\,(\zeta_c)$ ($M_\odot/L_{z\odot}$)
P1	2.33 ± 0.77	95 ± 35	2.81 ± 0.671	99 ± 27
P2	3.45 ± 0.73	62 ± 15	4.16 ± 0.67	70 ± 13
P3	2.01 ± 0.73	125 ± 68	2.84 ± 0.64	150 ± 44
P4	4.71 ± 0.76	113 ± 20	5.59 ± 0.68	123 ± 17
P5	2.48 ± 0.70	89 ± 31	3.17 ± 0.66	102 ± 25
P6	2.95 ± 0.78	242 ± 82	3.68 ± 0.68	224 ± 50

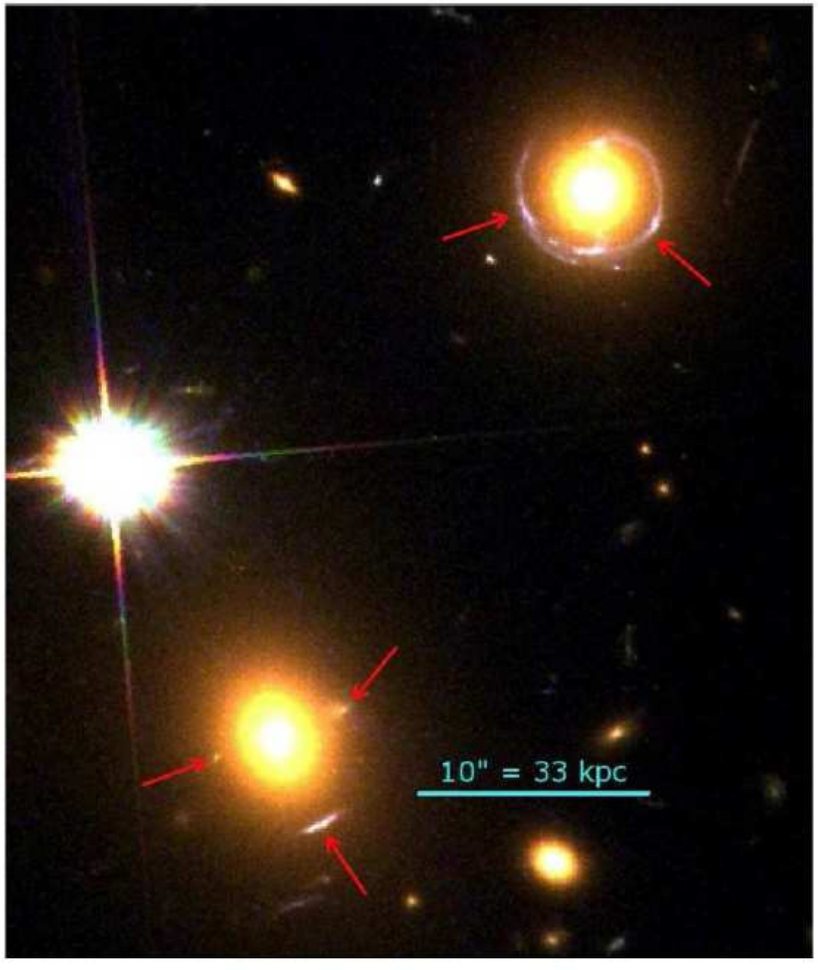

Shown in a color composite from the HST ACS images are the only two cases of strong lensing we detect in A520. Both sets of lenses are around giant elliptical galaxies located in structure 2, with the strong-lensing features marked by red arrows. Redshifts of the arcs are currently unknown.

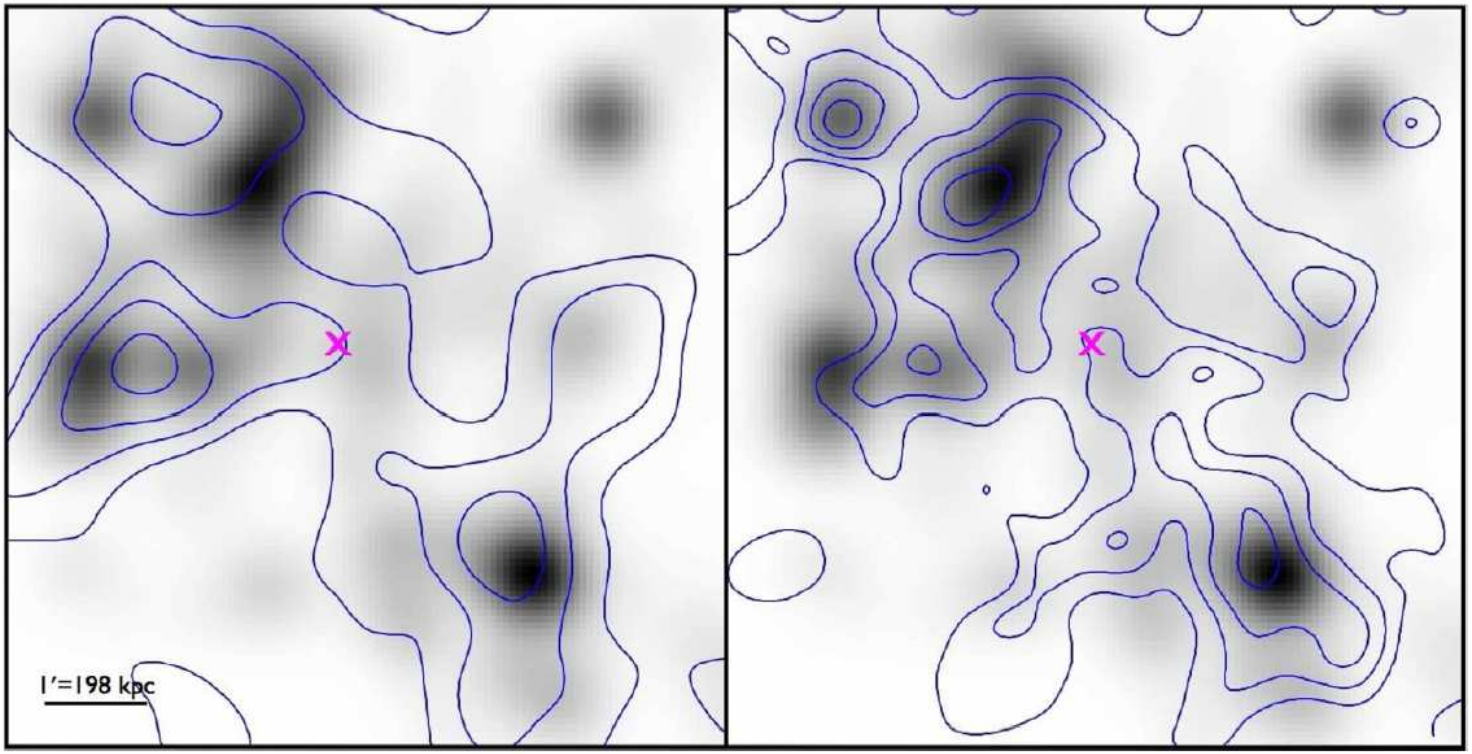

Weak-lensing surface density reconstructions using only the galaxies detected theMagellan image (left) and HST mosaic (right) as contours superimposed on the cluster galaxy luminosity in gray scale. The Magellan reconstruction has been smoothed by a 82 kpc Gaussian kernel, while the HST reconstruction was smoothed by a 26 kpc Gaussian kernel. The magenta $\times$ shows the location of the dark peak in J12.

Conclusions

- The mass structures in the reconstruction show excellent agreement with the distribution of light from cluster galaxies after subtraction of the mass of the intra-cluster X-ray plasma;
- While the masses we measure for the cluster overall and all of the cluster substructures containing galaxies are in good agreement with previous weak-lensing measurements in J12, we do not detect the mass overdensity spatially coincident with the X-ray plasma cloud that was found in both M07 and J12;
- The total mass in this region consistent with a constant mass-tolight ratio across the cluster, and exclude the additional mass in the central region at a $\sim$ 98% confidence level
- Using an aperture densitometry measurement instead of the mass reconstruction results in a slightly higher mass for the dark peak region ; it still excludes the mass from J12 at a 93% confidence level.
- We also find that the significances for the dark peak structure were overstated in both M07 and J12 as they calculated the significance by comparing their measured mass to a mass of 0 in the center of the cluster, and their significances of detection are $< 2\sigma$ and $\sim 2.3\sigma$, respectively, when measured compared with our constant mass-to-light ratio model.

Conclusions

- Several potential causes for the discrepancy in the central region between the various mass reconstructions while still having good agreement in the rest of the cluster core: the most likely explanation is an inherent alignment in the galaxies that were included in the J12 shear measurements but excluded from ours;.
- Regarding the discrepant mass-to-light ratio, we find that both M07 and J12 have significantly lower cluster luminosity measurements in the region of the ”dark peak” than our measurements, and this difference in cluster luminosity is responsible for the majority of the difference in the mass-to-light ratios for the central region between the studies.
- We identify one structure on the eastern edge of the HST image which has bright elliptical galaxies that are known to be part of the cluster for which neither we nor J12 obtain a significant amount of mass.
- However, we do detect mass in this region in a mass reconstruction shape measurements from the Magellan image. We are uncertain as to whether the lack of mass in this region is an aspect of the merger or an edge effect from the HST mosaic.

Conclusions

- The overall mass structure that we measure for A520 is in good agreement with a constant mass-to-light ratio, and therefore with collisionless CDM-similar to the conclusions drawn from all other well-studied merging clusters. Deriving a quantitative upper limit on the dark matter self-interaction crosssection from A520 will require additional kinematic information and detailed modeling of this merging system.